



Cite this: *Phys. Chem. Chem. Phys.*,
2016, **18**, 25546

Structure-dependent vibrational dynamics of $\text{Mg}(\text{BH}_4)_2$ polymorphs probed with neutron vibrational spectroscopy and first-principles calculations†

Mirjana Dimitrievska,^{*ab} James L. White,^c Wei Zhou,^b Vitalie Stavila,^c
Leonard E. Klebanoff^c and Terrence J. Udovic^b

The structure-dependent vibrational properties of different $\text{Mg}(\text{BH}_4)_2$ polymorphs (α , β , γ , and δ phases) were investigated with a combination of neutron vibrational spectroscopy (NVS) measurements and density functional theory (DFT) calculations, with emphasis placed on the effects of the local structure and orientation of the BH_4^- anions. DFT simulations closely match the neutron vibrational spectra. The main bands in the low-energy region (20–80 meV) are associated with the BH_4^- librational modes. The features in the intermediate energy region (80–120 meV) are attributed to overtones and combination bands arising from the lower-energy modes. The features in the high-energy region (120–200 meV) correspond to the BH_4^- symmetric and asymmetric bending vibrations, of which four peaks located at 140, 142, 160, and 172 meV are especially intense. There are noticeable intensity distribution variations in the vibrational bands for different polymorphs. This is explained by the differences in the spatial distribution of BH_4^- anions within various structures. An example of the possible identification of products after the hydrogenation of MgB_2 , using NVS measurements, is presented. These results provide fundamental insights of benefit to researchers currently studying these promising hydrogen-storage materials.

Received 25th June 2016,
Accepted 16th August 2016

DOI: 10.1039/c6cp04469g

www.rsc.org/pccp

Introduction

Complex-hydride systems must fulfill a wide range of requirements in order to function as hydrogen-storage materials. Among these, a high hydrogen content, fast kinetics of hydrogen desorption and absorption at a low operating temperature and pressure, as well as a high purity of the released hydrogen are the most important. Metal borohydrides ($\text{M}(\text{BH}_4)_x$) are considered as promising materials for hydrogen-storage applications due to their high volumetric and gravimetric hydrogen densities. $\text{M}(\text{BH}_4)_x$ are largely ionic compounds consisting of hydrogen-rich molecular BH_4^- anions counterbalanced by metal cations M^{x+} .

Magnesium borohydride ($\text{Mg}(\text{BH}_4)_2$) is a material currently undergoing intense scrutiny as a potential hydrogen-storage material. Among the alkali and alkaline-earth borohydrides, $\text{Mg}(\text{BH}_4)_2$ displays very interesting properties from both fundamental and applied perspectives.^{1–8} $\text{Mg}(\text{BH}_4)_2$ has a more favorable

thermodynamic stability in comparison to, *e.g.*, LiBH_4 , while still maintaining an attractive hydrogen-storage capacity of 14.9 mass%.¹ Additionally, $\text{Mg}(\text{BH}_4)_2$ in the bulk form has one of the lowest decomposition temperatures, and it is the only compound among the alkali and alkaline-earth borohydrides, which can be partially rehydrogenated under mild conditions (1–2 mass% at 210–285 °C and 100–155 bar).^{2–4} Total rehydrogenation from MgB_2 occurs only above 350 °C and at hydrogen pressures in excess of 800 bar, and results in a mixture of $\text{MgB}_{12}\text{H}_{12}$ and $\text{Mg}(\text{BH}_4)_2$.^{5–8} It has also been demonstrated that under mild temperature conditions (300 °C), $\text{Mg}(\text{BH}_4)_2$ is able to release up to 6 mass% gaseous products, the major component being hydrogen with only slight traces of diborane.^{4,9,10}

Understanding the evolution of the phases formed during the complex dehydrogenation process of $\text{Mg}(\text{BH}_4)_2$ has been the main goal of several previous studies.^{3,4,6,11} Although it was found that decomposition proceeds in multiple steps and is even partly reversible,^{12,13} the details of the decomposition mechanisms and the possible formation of the stable boron phases in the intermediate steps are still unclear. Most of the difficulties occurring in the identification of the decomposition intermediates arise from the amorphous nature of the final and intermediate compounds and of some of the high-temperature $\text{Mg}(\text{BH}_4)_2$ polymorphs. Indeed, $\text{Mg}(\text{BH}_4)_2$ is known for a variety of

^a National Renewable Energy Laboratory (NREL), 5013 Denver W Pkwy, Golden, CO 80401, USA. E-mail: mirjana.dimitrievska@nrel.gov

^b NIST Center for Neutron Research, National Institute of Standards and Technology, Gaithersburg, MD 20899-6102, USA. E-mail: mirjana.dimitrievska@nist.gov

^c Sandia National Laboratories, California P.O. Box 969, Livermore, CA 94551-0969, USA

† Electronic supplementary information (ESI) available. See DOI: 10.1039/c6cp04469g

possible structural polymorphs (both crystalline and amorphous), which have been either experimentally observed or theoretically predicted. Currently, six different crystalline polymorphs of $\text{Mg}(\text{BH}_4)_2$ have been reported: α ($P6_122$),¹⁴ β ($Fddd$),¹⁵ γ ($Ia\bar{3}d$),^{6,16} δ ($P4_2nm$),¹⁶ ϵ (no structural refinement)¹⁷ and ζ ($P3_112$).¹⁸ In order to understand the hydrogenation and dehydrogenation mechanisms in these materials properly, fundamental studies are necessary, especially related to the local structure of the BH_4^- anions as well as the global structure of different $\text{Mg}(\text{BH}_4)_2$ polymorphs.

Besides the intrinsic complexity of the decomposition process and the wide variety of the structural polymorphs, an existing discrepancy among the theoretically predicted and experimental results presents an additional issue for better understanding these materials. For example, only a few theoretical studies predict the experimentally reported $P6_122$ symmetry as a ground state for the α phase, while significantly more reports have proposed alternative structures.¹⁹ Similarly, first-principles calculations have shown that high-pressure δ -phase structures, such as $Fddd$,²⁰ $I4_1/acd$,²¹ or $I4_1/amd$,²² are more favorable than the reported $P4_2nm$ structure.¹⁶ The main reason for these discrepancies is the variety of equivalent crystalline symmetries of the $\text{Mg}(\text{BH}_4)_2$ polymorphs that are nearly degenerate in energy, as well as the dynamic effects that occur in these materials. As a consequence, this can lead to the incorrect assessment of the thermodynamic parameters, which in turn can affect the expected evolution of the hydrogen-storage properties of $\text{Mg}(\text{BH}_4)_2$. This is why agreement between the theoretical and experimental results is highly important, and is required to obtain high precision and accuracy with simulation methods.

In this regard, the main goal of this paper is to provide more detailed fundamental information regarding the structural and vibrational properties of different $\text{Mg}(\text{BH}_4)_2$ polymorphs (α , β , γ , and δ phases) from both theoretical and experimental points of view. Neutron vibrational spectroscopy (NVS) along with density functional theory (DFT) calculations are used in order to evaluate and explain the structure-dependent vibrational densities of states that are typical for each $\text{Mg}(\text{BH}_4)_2$ phase. Special focus is placed on the local structure and the orientation of the BH_4^- anions, which can be related to the stability of the different phases and can be easily probed using vibrational spectroscopy techniques.

Experimental

Materials synthesis

All $\text{Mg}(\text{BH}_4)_2$ samples contained natural boron. α - $\text{Mg}(\text{BH}_4)_2$ was synthesized using a slightly modified literature procedure²³ by reacting 50 mmol of $\text{Mg}(n\text{-Bu})_2$ (as a 1 mol l^{-1} solution in heptane, Sigma-Aldrich²⁴) with 190 mmol of $\text{BH}_3\cdot\text{S}(\text{CH}_3)_2$ (Sigma-Aldrich) as a solution in 100 mL of dry toluene. The reaction was performed under vigorous stirring at room temperature for 16 h followed by filtration. The white precipitate (the dimethylsulfide adduct of $\text{Mg}(\text{BH}_4)_2$) was washed with dry toluene and dried under vacuum at 150 °C for 24 h to remove $\text{S}(\text{CH}_3)_2$.

γ - $\text{Mg}(\text{BH}_4)_2$ was synthesized according to the procedure published by Filinchuk *et al.*,¹⁶ except that heating in a vacuum was performed at 90 °C. Finally, β - $\text{Mg}(\text{BH}_4)_2$ was obtained by heating α - $\text{Mg}(\text{BH}_4)_2$ at 190 °C in a dynamic vacuum for 16 h. The structure and crystal phases of the synthesized materials were confirmed by XRD measurements.

Characterization

The ¹⁰B isotope, a significant neutron absorber, comprises about 20% of natural boron. Hence, to maximize the neutron scattering signal, the $\text{Mg}(\text{BH}_4)_2$ powder samples were conformed to a thin flat-plate geometry, sealed into thin-walled Al cans, and measured in neutron reflection. All NVS measurements were performed at the National Institute of Standards and Technology (NIST) Center for Neutron Research (NCNR) on the Filter-Analyzer Neutron Spectrometer (FANS)²⁵ using the Cu(220) monochromator with pre- and post-collimations of 20' of arc in the case of reference samples and 60'–40' of arc in other cases, yielding a full-width-at-half-maximum energy (fwhm) resolution of about 3% and 5% of the neutron energy transfer, respectively. The spectra were collected by stepwise scanning the incident neutron energy with a fixed final energy of 1.2 meV.

Theoretical calculations

First-principles calculations were performed within the plane-wave implementation of the generalized gradient approximation to density functional theory (DFT) using a Vanderbilt-type ultrasoft potential with Perdew–Burke–Ernzerhof exchange correlation.²⁶ A cutoff energy of 544 eV and a relatively dense k -point mesh (generated using the Monkhorst–Pack scheme) were used and found to be enough for the total energy to converge within 0.01 meV per atom. For comparison with the NVS measurements, the phonon densities of states (PDOSs) were calculated from the DFT-optimized structure using the supercell method with finite displacements^{27,28} and were appropriately weighted to take into account the H, Mg, and B total neutron scattering cross sections. NVS was computed within the incoherent approximation, and we used the well-known rigorous schemes²⁹ for both one phonon and one + two phonon processes.

All structural depictions were made using the VESTA (visualization for electronic and structural analysis) software.³⁰ For all figures, standard uncertainties are commensurate with the observed scatter in the data, if not explicitly designated by vertical error bars.

Results and discussion

$\text{Mg}(\text{BH}_4)_2$ polymorphs: structural comparisons

Depending on the synthesis conditions, $\text{Mg}(\text{BH}_4)_2$ can crystallize in different phases, which have been determined using X-ray diffraction (XRD) and neutron diffraction techniques.¹² This study is focused on the α , β , γ , and δ phases of $\text{Mg}(\text{BH}_4)_2$. There are significant differences among the ionic arrangement of the different $\text{Mg}(\text{BH}_4)_2$ polymorphs, whose crystal structures can be seen in Fig. 1.

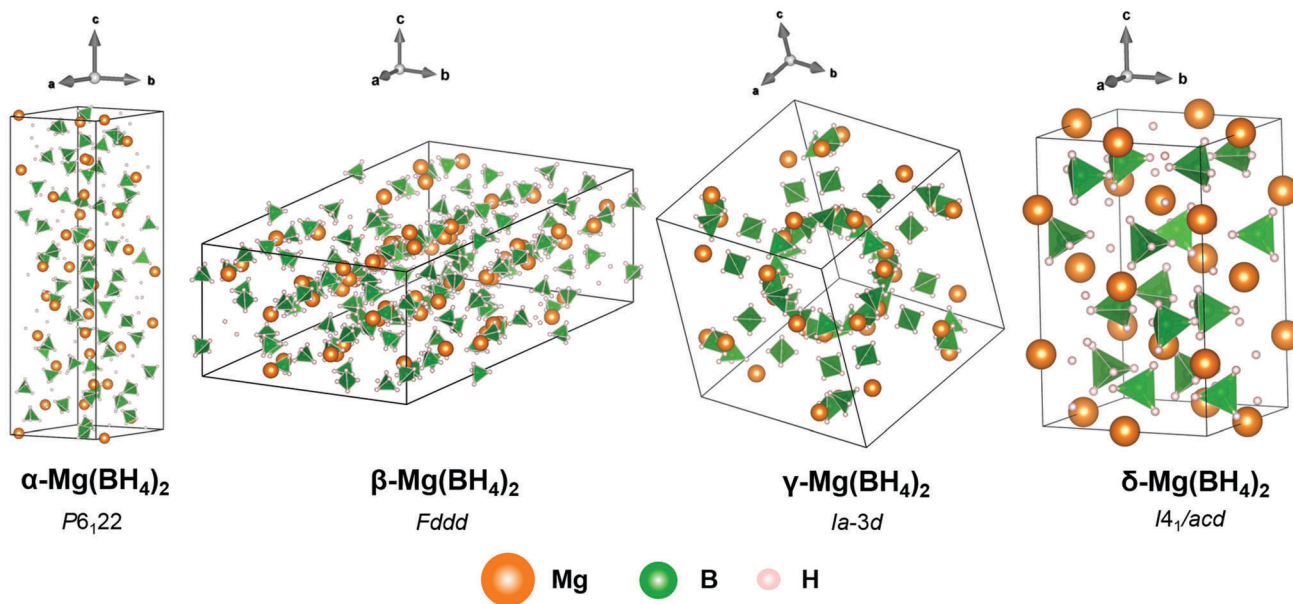


Fig. 1 Reported crystal structures of the α , β , γ and δ phases of $\text{Mg}(\text{BH}_4)_2$. Mg atoms are shown as orange spheres, BH_4 groups as green tetrahedra, and unit cells are defined by black lines.

The α phase is characterized by a complex hexagonal lattice which belongs to the $P6_122$ space group. It is built from MgH_8 polyhedra almost linearly coordinated by H_2BH_2 units and organized into a 3D network by five-membered $(-\text{Mg}-\text{BH}_4^-)_n$ rings.³¹ On the other hand, the β phase is formed from two different MgH_8 polyhedra coordinated by $(-\text{Mg}-\text{BH}_4^-)_n$ rings, for which the n indices cannot assume odd values. This results in an orthorhombic primitive cell with $Fddd$ symmetry.¹⁴ The main difference between the α and β phases originates from the shape of the MgH_8 polyhedra.

In the case of the α phase, MgH_8 polyhedra have the shape of a snub disphenoid (J_{84} in Johnson notation³²), while for the β phase, there are two different shapes of the MgH_8 polyhedra: one Mg atom forms the biagumented triangular prism (J_{50}) and the other forms gyrobifastigium (J_{26}).¹⁶ The γ phase has a highly symmetric cubic structure with the $Ia\bar{3}d$ space group, where a single Mg site has a tetrahedral environment of BH_4 groups. This results in a 3D-network of interconnected channels, making this structure highly porous (the empty volume in the structure amounts to 33%).¹⁶

Finally, the δ phase was originally reported to have a tetragonal structure ($P4_2nm$) consisting of two interpenetrating $\text{Mg}(\text{BH}_4)_2$ frameworks, where each framework resembles the cristobalite structure (a polymorph of SiO_2), while their doubly interpenetrated arrangement has a Cu_2O topology.¹⁶ As to allude to earlier, first-principles calculations indicate that this structure is dynamically unstable leading to negative phonon modes.²¹ In contrast, among the variety of a stable, lower-energy candidates, the calculated highest-symmetry $I4_1/acd$ structure²¹ (also consistent with the reported XRD results) is likely closer to reality.

$\text{Mg}(\text{BH}_4)_2$ polymorphs: neutron vibrational spectroscopy and first-principles calculations

In order to compare the vibrational properties of the different $\text{Mg}(\text{BH}_4)_2$ polymorphs, NVS measurements were performed on

the α -, β - and γ - $\text{Mg}(\text{BH}_4)_2$ phases at 4 K, for which the representative spectra are shown in Fig. 2. The high-density δ - $\text{Mg}(\text{BH}_4)_2$ phase was not made in a significant enough amount to measure a good vibrational spectrum at this time.

It should be noted that in comparison to the Raman and infrared (IR) measurements where only the Γ -point phonons are observed, NVS probes the full first Brillouin zone of the crystal, resulting in the observation of lattice modes which are averaged over their full dispersion curves. Moreover, the selection-rule restrictions for Raman and IR absorptions as imposed by the dipole and polarizability approximations are absent in NVS, meaning that all possible vibrational modes can be observed in the spectra. Furthermore, as the total neutron scattering cross section for H is relatively large compared to the Mg and B, each spectrum reflects a hydrogen-weighted PDOS dominated by the optical phonons involving large-amplitude H motions, namely, BH_4^- modes. This renders NVS a very suitable technique for probing the local structure of the BH_4^- anions.

Several intense bands are observed in the low-energy region from 20 to 80 meV ($1 \text{ meV} \approx 8.066 \text{ cm}^{-1}$) in Fig. 2, which correspond to the BH_4^- librational (torsional) modes, and are not usually observed in Raman spectra.³¹ Moving to higher energy-transfer values, broad band features are observed in the 80–120 meV region, which are attributed to the overtone and combination bands originating from the lower-energy modes. Furthermore, a number of sharp peaks are noticeable in the 120–190 meV region, of which four peaks centered at around 140, 142, 160, and 172 meV are particularly intense.

According to group-theory calculations, BH_4^- anions have a high tetrahedral (T_d) symmetry for which the irreducible representation in the Mulliken notation can be written as $\Gamma = A_1 \oplus E \oplus 2F_2$.

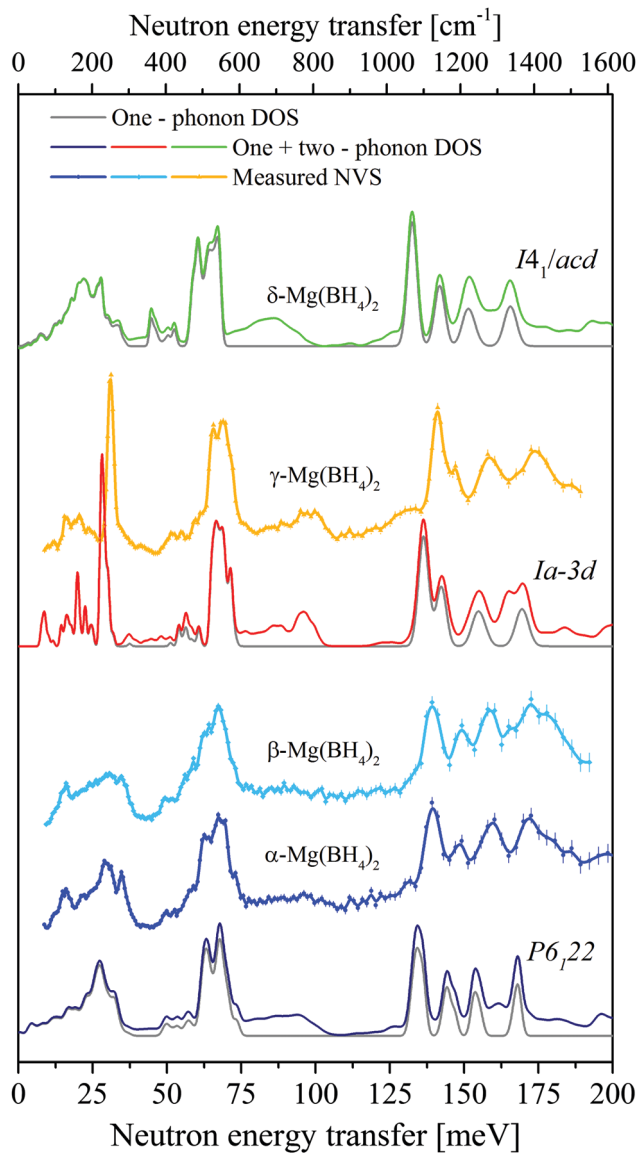


Fig. 2 Neutron vibrational spectra of the α -, β - and γ -Mg(BH₄)₂ phases at 4 K compared to the simulated one-phonon and one + two-phonon densities of states from first-principles phonon calculations of the DFT-optimized 0 K structures. Additional simulated one-phonon and one + two-phonon densities of states of the supposed $I4_1/acd$ δ -phase structure are included for comparison. *N.B.*: the experimental NVS spectra of α - and β -Mg(BH₄)₂ phases (dark and light blue lines labeled as α -Mg(BH₄)₂ and β -Mg(BH₄)₂, respectively) should be compared to the one + two-phonon DOS (dark blue line labeled as $P6_122$), while the NVS spectra of γ -Mg(BH₄)₂ phase (orange line labeled as γ -Mg(BH₄)₂) should be compared to the one + two-phonon DOS (red line labeled as $Ia\bar{3}d$).

In this case, A₁ and E symmetry modes correspond to the symmetric stretching and bending vibrations of the H atoms, respectively, while one of the F₂ modes corresponds to the asymmetric stretching and the other F₂ mode to asymmetric bending vibrations. Here the A modes are non-degenerate, while the E modes are doubly degenerate, and the F modes are triply degenerate, and according to the selection rules, all modes are Raman-active, while only the F₂ modes are additionally IR-active.

Having in mind this notation and comparing the results with the DFT simulations, the very intense peaks observed in the 80–190 meV region could be resolved as follows: the peaks observed at 140 and 142 meV correspond to the asymmetric bending vibrations (F₂ symmetry mode), while the peaks at 160 and 170 meV are attributed to the symmetric bending vibrations (E symmetry mode). The positions of the peaks are also in good agreement with the results obtained from Raman and IR spectroscopy.^{12,31} Vibrational patterns of the librational, bending, and stretching modes of the BH₄[−] anions obtained from the DFT simulations are illustrated in Fig. 3, while animations of the complete motion for vibrational modes of all discussed phases are presented in the ESI.†

Fig. 2 also compares the neutron vibrational spectra for the α - and γ -Mg(BH₄)₂ phases with the simulated PDOSs computed from the experimentally observed structures after DFT optimization. The theoretical results also include the PDOS of the supposed $I4_1/acd$ δ phase structure, which was not experimentally measured. Ignoring the expected minor inaccuracies with DFT in predicting absolute band energies, there is a good overall qualitative agreement between experiment and theory for α and γ phases. Although within 5 to 10% shifts in mode frequencies compared to experimental values are typical using state-of-the-art DFT functionals, we note that the relative frequencies of the entire simulated spectra are seen to be in very good overall agreement with what is measured. In particular, the simulated one + two phonon density of states reproduces the general details of the librational band lineshapes (which vary among the three phases), the complex-band structure of the bending modes, and the broad combination bands. No attempt was made to calculate the PDOS of β -Mg(BH₄)₂, since this is a disordered phase, and one would need to construct an appropriately large supercell to mimic such disorder. Yet, it is clear from comparing the structural details and measured PDOSs of α - and β -Mg(BH₄)₂ that there are considerable local structural similarities between the two.

It should be noted that, in the case of the δ phase, DFT calculations of the PDOS using the previously reported $P4_2nm$ symmetry confirmed dynamical instability, with some of the modes having significantly negative frequencies. In contrast, the alternative optimized $I4_1/acd$ -symmetric structure²¹ indeed proved to be dynamically stable, yielding the simulated PDOS in Fig. 2. The CIF and animation files for the optimized $I4_1/acd$ structure are provided in the ESI.† This $I4_1/acd$ structure is also in agreement with the reported XRD data of the δ -phase and almost identical to the pattern of the $P4_2nm$ structure, since both possess similar Mg and B positions.

Deviations between the two structures mainly involve the relative positions of the H atoms (*i.e.*, the orientations of the BH₄[−] anions). Nonetheless, we cannot corroborate that the former structure is closer to the actual high-pressure δ -phase structure without additional neutron diffraction and vibrational spectroscopy measurements, which are much more sensitive to hydrogen atom locations and displacements.

Probably one of the more interesting features of the α -, β -, and γ -Mg(BH₄)₂ spectra is the observed bimodal distribution of

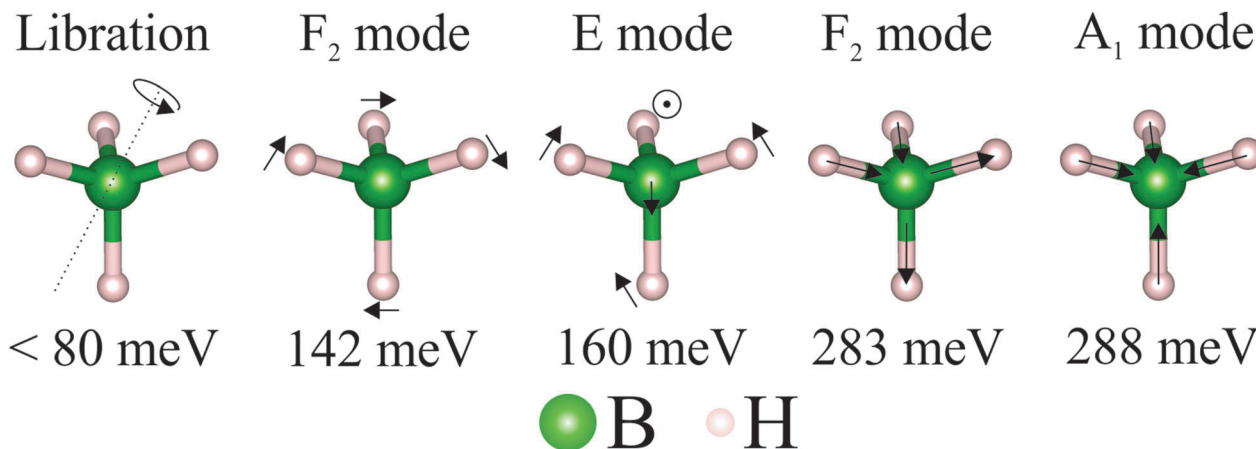


Fig. 3 Atomic displacements of the different vibrational modes characteristic of the BH_4^- anions in the $\text{Mg}(\text{BH}_4)_2$ polymorphs. Rotational arrows denote the direction of movement of the corresponding atoms.

librational band intensities centered near 35 and 70 meV. In contrast, the simulated $\delta\text{-Mg}(\text{BH}_4)_2$ spectrum deviates somewhat from this behavior, with the lower intensity band redshifted closer to 25 meV. In all $\text{Mg}(\text{BH}_4)_2$ structures, despite their different symmetries, the BH_4^- anions more or less orient themselves with two of their four H atoms (*i.e.*, a BH_4^- tetrahedron edge) directed towards (straddling) their nearest-neighbor Mg^{2+} cations. Fig. 4 illustrates such an arrangement for $\gamma\text{-Mg}(\text{BH}_4)_2$. The DFT phonon calculations for the α -, γ - and $\delta\text{-Mg}(\text{BH}_4)_2$ phases and resulting mode simulations that can be generated from the ESI[†] animation files indicate the differences in the types of modes responsible for this bimodal band. These differences are best described with reference to Fig. 4.

In general, for all phases, the much softer librational band is found to be dominated by the BH_4^- librational motions around the x -axis (which is drawn parallel to the Mg–B alignment). The higher-energy librational band centered near 70 meV is found to be dominated by combinations of librational motions around the orthogonal y - and z -axes. From the perspective of the Mg^{2+} cations, one might describe the x -type librational motions of the two near-neighbor H atoms as H–H torsions, and y - and z -type librational motions as wags and rocks. It is clear that the torsional variety of librations experiences a much softer rotational potential than the wagging and rocking varieties. It should be

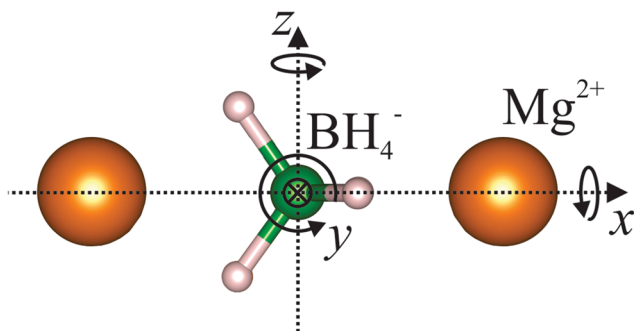


Fig. 4 Orientation of the BH_4^- anions and possible librational motions in the $\gamma\text{-Mg}(\text{BH}_4)_2$ phase.

noted that the porous, cubic $\gamma\text{-Mg}(\text{BH}_4)_2$ phase displays narrower individual librational bands (especially the softer band) than the other denser phases, signaling more degeneracies (less dispersion) in the various related normal modes. These less dispersed bands are likely explained by consequences of both the cubic lattice symmetry and less degeneracy-breaking, near-neighbor interactions due to the relative lower density of the γ -phase structure.

It should be pointed out that these measured neutron vibration spectra of different $\text{Mg}(\text{BH}_4)_2$ phases can potentially be used as signatures/references marking the presence of a particular polymorph, especially in cases where the XRD patterns show amorphous-like structures or where the material is present in non-bulk-like, nanocrystalline forms.

Additionally, as the DFT-simulated spectra were observed to match well the experimental results of the α and γ polymorphs, we are reasonably confident that DFT-simulated spectra of other possible polymorphs that are difficult or impossible to measure experimentally in pure form, such as the one for the δ phase in Fig. 2 (which shows some notable differences compared to the other polymorphs), will sufficiently reproduce the expected PDOSs and can be used without measured reference spectra to help identify the presence of these polymorphs in a material of unknown structure.

Fig. 5 shows an example of possible phase identification using NVS for a sample synthesized after 7 d of hydrogenation of MgB_2 at 380 °C and 700 bar H_2 . Upon comparing the measured spectrum to the different $\text{Mg}(\text{BH}_4)_2$ phase standards (as shown in Fig. 5), the PDOS of the hydrogenated sample resembles those of the α - and $\beta\text{-Mg}(\text{BH}_4)_2$ phases but clearly displays some additional scattering intensity that is contributing to the PDOS at energies above the BH_4^- librational bands.

The additional spectral intensity from this component is consistent with that of $\text{B}_{12}\text{H}_{12}^{2-}$ anions³⁴ (Fig. 5) which are known to form during the hydrogenation of magnesium diboride.^{7,8} Yet, at this point, we cannot rule out the possible spectral signatures of other B_xH_y -type intermediate species present, such as $\text{B}_{10}\text{H}_{10}^{2-}$ anions^{35,36} or other borohydride cluster species, without further

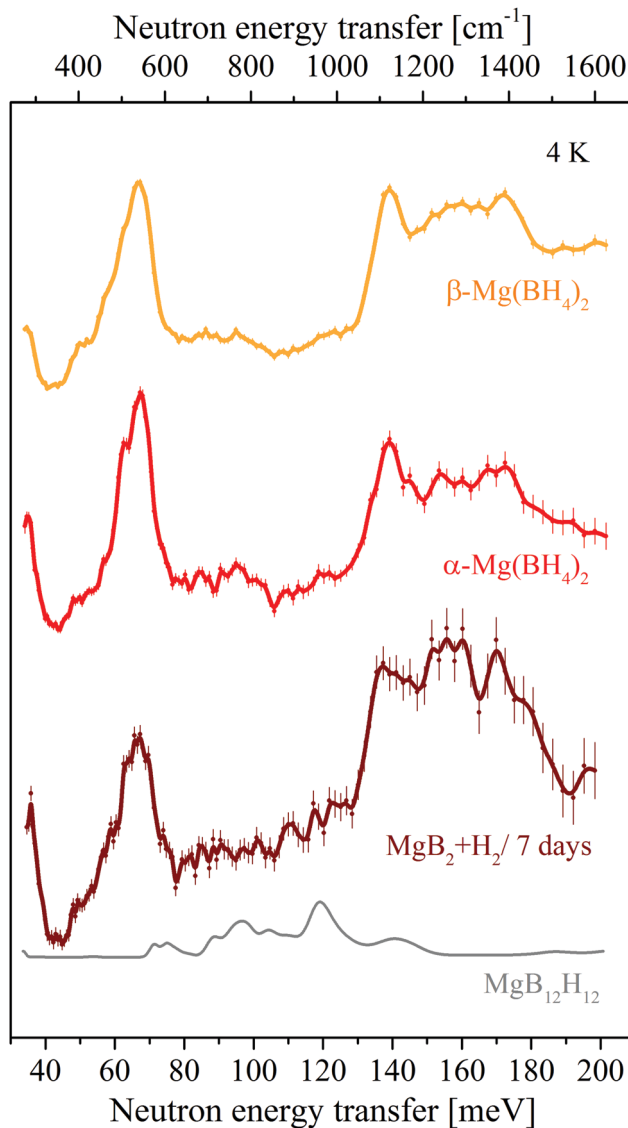


Fig. 5 Neutron vibrational spectrum of the $\text{Mg}(\text{BH}_4)_2$ phase formed after 7 d of hydrogenation of MgB_2 at 380 °C and 700 bar H_2 compared to those for the α - and β - $\text{Mg}(\text{BH}_4)_2$ phases and the simulated one + two-phonon density of states of $\text{MgB}_{12}\text{H}_{12}$ obtained from first-principles phonon calculations of the DFT-optimized 0 K structure predicted from theory.³³ N.B., all spectra were measured at lower instrumental resolution than in Fig. 2.

analysis by another complementary technique such as NMR. Further investigations about the hydrogenation process of MgB_2 and its products are currently underway in our labs.

Conclusions

NVS and DFT calculations were utilized in order to gain deeper insights into the structure-dependent vibrational properties of the α -, β -, γ -, and δ - $\text{Mg}(\text{BH}_4)_2$ phases. DFT simulations closely match the experimental data and the combined study shows that there are minor but noticeable changes in the hydrogen-weighted PDOSS for the different phases.

The low-energy region (20–80 meV) of the spectra is characterized by the librational modes, while the intermediate region (80–120 meV) is attributed to the combination and overtone bands, and the high-energy region (120–200 meV) corresponds to the peaks attributed to the symmetric and asymmetric bending vibrations, of which four peaks centered at around 140, 142, 160, and 172 meV are especially intense. Intensity distribution variations observed among the spectra of the different polymorphs are explained by the changes in the spatial distribution of BH_4^- anions within these various structures. The measured neutron vibration spectra of the different $\text{Mg}(\text{BH}_4)_2$ phases can be used as references to help identify the presence of a particular polymorph in materials of the unknown structure. Additionally, the good agreement observed between DFT simulations and experimental results gives us confidence that first-principles calculations can accurately describe the bonding in other $\text{Mg}(\text{BH}_4)_2$ polymorphs yet to be successfully measured in pure form. Thus, it is possible that simulated spectra by themselves of such polymorphs can be used to identify their presence in neutron vibrational spectra of future composite materials containing $\text{Mg}(\text{BH}_4)_2$.

Overall, these results provide valuable insights into the phase dynamics in $\text{Mg}(\text{BH}_4)_2$, for which a deeper fundamental understanding is beneficial for determining the potential of this material for practical hydrogen-storage applications.

Acknowledgements

Sandia National Laboratories is a multi-program laboratory managed and operated by Sandia Corporation, a wholly owned subsidiary of Lockheed Martin Corporation, for the U.S. Department of Energy's National Nuclear Security Administration under contract DE-AC04-94AL85000. M. D. gratefully acknowledges research support from the U.S. Department of Energy, Office of Energy Efficiency and Renewable Energy, Fuel Cell Technologies Office, under Contract No. DE-AC36-08GO28308.

References

- 1 Y. Nakamori, K. Miwa, A. Ninomiya, H. Li, N. Ohba, S. Towata, A. Züttel and S. Orimo, *Phys. Rev. B: Condens. Matter Mater. Phys.*, 2006, **74**, 45126.
- 2 O. Zavorotynska, I. Saldan, S. Hino, T. D. Humphries, S. Deledda and B. C. Hauback, *J. Mater. Chem. A*, 2015, **3**, 6592–6602.
- 3 I. Saldan, S. Hino, T. D. Humphries, O. Zavorotynska, M. Chong, C. M. Jensen, S. Deledda and B. C. Hauback, *J. Phys. Chem. C*, 2014, **118**, 23376–23384.
- 4 M. Chong, A. Karkamkar, T. Autrey, S. Orimo, S. Jalisatgi and C. M. Jensen, *Chem. Commun.*, 2011, **47**, 1330–1332.
- 5 M. P. Pitt, C. J. Webb, M. Paskevicius, D. Sheptyakov, C. E. Buckley and E. M. Gray, *J. Phys. Chem. C*, 2011, **115**, 22669–22679.
- 6 J. G. Vitillo, S. Bordiga and M. Baricco, *J. Phys. Chem. C*, 2015, **119**, 25340–25351.

- 7 G. Severa, E. Rönnebro and C. M. Jensen, *Chem. Commun.*, 2010, **46**, 421–423.
- 8 R. J. Newhouse, V. Stavila, S.-J. Hwang, L. E. Klebanoff and J. Z. Zhang, *J. Phys. Chem. C*, 2010, **114**, 5224–5232.
- 9 E. Albanese, G. N. Kalantzopoulos, J. G. Vitillo, E. Pinatel, B. Civalleri, S. Deledda, S. Bordiga, B. C. Hauback and M. Baricco, *J. Alloys Compd.*, 2013, **580**(Supplement 1), S282–S286.
- 10 K. Chłopek, C. Frommen, A. Léon, O. Zabara and M. Fichtner, *J. Mater. Chem.*, 2007, **17**, 3496–3503.
- 11 C. J. Sahle, S. Kujawski, A. Remhof, Y. Yan, N. P. Stadie, A. Al-Zein, M. Tolan, S. Huotari, M. Krisch and C. Sternemann, *Phys. Chem. Chem. Phys.*, 2016, **18**, 5397–5403.
- 12 O. Zavorotynska, A. El-Kharbachi, S. Deledda and B. C. Hauback, *Int. J. Hydrogen Energy*, 2016, **41**, 14387–14403.
- 13 O. Zavorotynska, S. Deledda and B. C. Hauback, *Int. J. Hydrogen Energy*, 2016, **41**, 9885–9892.
- 14 Y. Filinchuk, R. Černý and H. Hagemann, *Chem. Mater.*, 2009, **21**, 925–933.
- 15 J.-H. Her, P. W. Stephens, Y. Gao, G. L. Soloveichik, J. Rijssenbeek, M. Andrus and J.-C. Zhao, *Acta Crystallogr., Sect. B: Struct. Sci.*, 2007, **63**, 561–568.
- 16 Y. Filinchuk, B. Richter, T. R. Jensen, V. Dmitriev, D. Chernyshov and H. Hagemann, *Angew. Chem., Int. Ed.*, 2011, **50**, 11162–11166.
- 17 M. Paskevicius, M. P. Pitt, C. J. Webb, D. A. Sheppard, U. Filsø, E. M. Gray and C. E. Buckley, *J. Phys. Chem. C*, 2012, **116**, 15231–15240.
- 18 B. Richter, D. B. Ravnsbæk, N. Tumanov, Y. Filinchuk and T. R. Jensen, *Dalton Trans.*, 2015, **44**, 3988–3996.
- 19 A. Bil, B. Kolb, R. Atkinson, D. G. Pettifor, T. Thonhauser and A. N. Kolmogorov, *Phys. Rev. B: Condens. Matter Mater. Phys.*, 2011, **83**, 224103.
- 20 J. Fan, D. Duan, X. Jin, K. Bao, B. Liu and T. Cui, *J. Chem. Phys.*, 2013, **138**, 214503.
- 21 X.-F. Zhou, A. R. Oganov, G.-R. Qian and Q. Zhu, *Phys. Rev. Lett.*, 2012, **109**, 245503.
- 22 J. Fan, K. Bao, D.-F. Duan, L.-C. Wang, B.-B. Liu and T. Cui, *Chin. Phys. B*, 2012, **21**, 86104.
- 23 P. Zanella, L. Crociani, N. Masciocchi and G. Giunchi, *Inorg. Chem.*, 2007, **46**, 9039–9041.
- 24 The mention of all commercial suppliers in this paper is for clarity. This does not imply the recommendation or endorsement of these suppliers by NIST.
- 25 T. J. Udovic, C. M. Brown, J. B. Leão, P. C. Brand, R. D. Jiggetts, R. Zeitoun, T. A. Pierce, I. Peral, J. R. D. Copley, Q. Huang, D. A. Neumann and R. J. Fields, *Nucl. Instrum. Methods Phys. Res., Sect. A*, 2008, **588**, 406–413.
- 26 P. Giannozzi, S. Baroni, N. Bonini, M. Calandra, R. Car, C. Cavazzoni, D. Ceresoli, G. L. Chiarotti, M. Cococcioni, I. Dabo, A. D. Corso, S. de Gironcoli, S. Fabris, G. Fratesi, R. Gebauer, U. Gerstmann, C. Gougoussis, A. Kokalj, M. Lazzeri, L. Martin-Samos, N. Marzari, F. Mauri, R. Mazzarello, S. Paolini, A. Pasquarello, L. Paulatto, C. Sbraccia, S. Scandolo, G. Sclauzero, A. P. Seitsonen, A. Smogunov, P. Umari and R. M. Wentzcovitch, *J. Phys.: Condens. Matter*, 2009, **21**, 395502.
- 27 G. Kresse, J. Furthmüller and J. Hafner, *EPL*, 1995, **32**, 729.
- 28 T. Yildirim, *Chem. Phys.*, 2000, **261**, 205–216.
- 29 G. L. Squires, *Introduction to the Theory of Thermal Neutron Scattering*, Cambridge University Press, 2012.
- 30 K. Momma and F. Izumi, *J. Appl. Crystallogr.*, 2011, **44**, 1272–1276.
- 31 A. Giannasi, D. Colognesi, L. Ulivi, M. Zoppi, A. J. Ramirez-Cuesta, E. G. Bardají, E. Roehm and M. Fichtner, *J. Phys. Chem. A*, 2010, **114**, 2788–2793.
- 32 N. W. Johnson, *Can. J. Math.*, 1966, **18**, 169–200.
- 33 V. Ozolins, E. H. Majzoub and C. Wolverton, *J. Am. Chem. Soc.*, 2009, **131**, 230–237.
- 34 N. Verdál, W. Zhou, V. Stavila, J.-H. Her, M. Yousufuddin, T. Yildirim and T. J. Udovic, *J. Alloys Compd.*, 2011, **509**(suppl 2), S694–S697.
- 35 H. Wu, W. S. Tang, V. Stavila, W. Zhou, J. J. Rush and T. J. Udovic, *J. Phys. Chem. C*, 2015, **119**, 6481–6487.
- 36 H. Wu, W. S. Tang, W. Zhou, V. Stavila, J. J. Rush and T. J. Udovic, *CrystEngComm*, 2015, **17**, 3533–3540.